Fuel 416 (2026) 138474

Contents lists available at ScienceDirect

Fuel

journal homepage: www.elsevier.com/locate/jfue

Full length article

Generation and stability of bulk nanobubbles in liquid fuel and their influence on spray characteristics

Abinash Biswal[a,*], Suraj Prashad Sharma[a], Roger Cracknell[b], Hua Zhao[a], Xinyan Wang[a]

[a] Centre for Advanced Powertrain and Fuels, Brunel University of London, London, England, UK
[b] Shell Global Solutions (UK) Ltd., London, UK

HIGHLIGHTS

- Stable air nanobubbles in gasoline produced via hydrodynamic cavitation.
- Initial concentration of 5.12×10^{11} nanobubble/mL with ~35 nm mean size was achieved.
- Air nanobubbles remained stable in gasoline for over 120 days.
- Nanobubbles reduced spray penetration and enhanced atomization.
- ANB fuel showed lower droplet velocity and a uniform size distribution.

ARTICLE INFO

Keywords:
Nanobubbles
Zeta potential
GDI spray
Diffused back illumination
PDA

ABSTRACT

Nanobubbles have attracted increasing attention due to their unique physicochemical properties; however, their application in fuel and combustion research remains limited. This study investigates the generation of air nanobubbles (ANBs) in gasoline and their influence on spray characteristics in gasoline direct injection (GDI) systems. ANBs were produced using a custom-designed hydrodynamic cavitation generator incorporating a zero-clearance pump. Dynamic light scattering and nanoparticle tracking analysis demonstrated the formation of a highly concentrated nanobubble population (5.12×10^{11} particles/mL), with diameters ranging from 40 to 200 nm and a negative zeta potential between −20 and −25 mV, indicating good stability in gasoline. Spray behavior of ANB-enriched gasoline was evaluated in a constant-volume chamber using a single-hole GDI injector at injection pressures of 50, 100, and 150 bar. Diffused back illumination technique was employed to analyze macroscopic spray characteristics, while phase Doppler anemometry was used to measure droplet size and axial velocity distributions. Compared to baseline gasoline, ANB fuel exhibited consistently shorter penetration lengths, smoother spray boundaries, and lower spray density factors, suggesting improved atomization and air–fuel mixing. PDA measurements further revealed reduced axial droplet velocities, attributed to enhanced secondary breakup associated with nanobubble dynamics. These findings demonstrate that air nanobubbles can significantly influence spray development in GDI systems, offering a promising approach for improving fuel atomization and supporting the development of advanced, high-efficiency combustion technologies.

1. Introduction

Nanobubbles and microbubbles have become a prominent area of research due to their exceptional performance across various applications, including water treatment, flotation techniques, surface cleaning, and medical uses such as drug delivery. However, most of the research is still in the laboratory phase, with potential for market adoption in the near future [1–5]. Nanobubbles (NBs) are sub-micrometer gas-filled cavities, typically less than 200 nm in diameter, that exhibit remarkable stability in liquid mediums due to their unique physical and chemical properties [5–7]. Unlike conventional bubbles, which rise and collapse rapidly due to buoyancy, nanobubbles exhibit Brownian motion and can remain suspended for extended periods. This stability is attributed to their high internal pressure, zeta potential, and strong interfacial adsorption forces. Over the past two decades, nanobubbles have gained increasing attention across diverse applications, including biomedical engineering, water treatment, agriculture, and environmental remediation [5,7–9].

* Corresponding author.
Email address: Abinash.Biswal@brunel.ac.uk (A. Biswal).

https://doi.org/10.1016/j.fuel.2026.138474
Received 16 August 2025; Received in revised form 12 January 2026; Accepted 18 January 2026
Available online 29 January 2026

Nomenclature

ANB	Air nanobubbles
DBI	Diffused back illumination
D32 / SMD	Sauter mean diameter
Di	Individual droplet diameter
DLS	Dynamic light scattering
fps	Frames per second
GDI	Gasoline direct injection
I_i	Intensity of the ith pixel (background subtracted image)
I_{max}	Maximum possible pixel intensity value
NB	Nanobubbles
n	Total number of pixels within the detected spray area
NTA	Nanoparticle tracking analysis
Pa	Ambient pressure
PDA	Phase Doppler anemometry
Pi	Internal pressure of a nanobubble
RI	Spray irregularity index
SDF	Spray density factor
SOI	Start of injection
ST	Surface tension of fuel
Vi	Individual droplet axial velocity
Vm	Mean droplet axial velocity

However, their potential in fuel and combustion research remains largely unexplored.

Nanobubbles possess distinct physicochemical properties that set them apart from larger bubbles. Their small size results in a high surface area-to-volume ratio, which enhances their interaction with the surrounding medium. Additionally, nanobubbles exhibit high internal gas pressure, which theoretically should lead to rapid dissolution based on the Epstein-Plesset theory [10–12]. However, experimental studies have shown that bulk nanobubbles can persist in liquid for weeks or even months, challenging classical thermodynamic predictions. Several hypotheses have been proposed to explain this stability, including electrostatic repulsion due to high zeta potential, gas supersaturation, and the formation of a compressed amphiphilic monolayer around the bubbles. These factors collectively contribute to the prolonged existence of nanobubbles in liquid fuels [12]. Recent molecular dynamics (MD) simulations conducted by our research group [13–15] have explored the fundamental behavior of gas nanobubbles in liquid fuels such as iso-octane, dodecane, and methanol. These studies revealed that the interactions between gas and liquid molecules play a critical role in nanobubble formation and their resulting physical properties, highlighting the potential influence of nanobubbles on fuel injection and combustion processes.

Gasoline Direct Injection (GDI) engines have become a dominant technology in modern automotive applications due to their superior fuel efficiency and lower emissions compared to conventional port fuel injection (PFI) engines [16]. In a GDI system, high-pressure fuel injection directly into the combustion chamber allows for finer atomization, improved air-fuel mixing, and better combustion control [17,18]. In this context, integrating nanobubbles into liquid fuels presents an innovative approach to enhance fuel-air mixing, alter spray characteristics, and potentially improve combustion performance.

The relevant research on fuel injection with nanobubbles is very limited, creating a significant opportunity for further exploration. Oh et al. [19,20] conducted the first study to generate bulk hydrogen nanobubbles in gasoline using a nanoporous membrane method, and also examined their long-term stability. The study, conducted at a constant temperature of 298.15 K for 121 days, found that hydrogen nanobubbles remained stable with a mean diameter of 159 ± 31.91 nm and a concentration of $11.25 \pm 2.77\times10^8$ immediately after generation. The mean diameter showed no significant change over time. Additionally, the ζ-potential was found to be -30 mV, confirming the stability of the hydrogen nanobubbles. Furthermore, Oh et al. [20] investigated the impact of hydrogen nanobubbles in an IC engine using a laboratory engine. The results showed an increase in power output by up to 4%, reaching 27 KW (compared to 25.96 KW for conventional gasoline) at 40% engine load. Under the same conditions, the brake-specific fuel consumption (BSFC) decreased from 291.10 g/KWh to 269.48 g/KWh.

In another study, Nakatake et al. [21] created air nanobubbles in gas oil and tested them in a diesel engine. The nanobubbles had a size range of 100 nm to 200 nm, with a concentration of approximately 0.5×10^8 bubbles/ml. The results indicated a reduction in fuel consumption by 3.2% under average load and 6.2% under maximum load. Additionally, the nanobubble-treated gas oil improved charging efficiency, exhaust gas temperature, smoke, and engine noise by approximately 1% at maximum load. Gobinath et al. [22] investigated air nanobubble-enhanced combustion in a common rail direct injection (CRDI) engine using mustard biodiesel. Their findings revealed a 25% reduction in brake-specific fuel consumption and significant reductions in NOx and CO emissions.

Despite the limited number of reactive studies mentioned above, only one non-reactive optical study has been conducted recently in 2024 [23]. In this study, a premix of micro-nano bubbles of air was prepared in diesel, and fundamental spray injection tests were carried out in a constant volume chamber. The study demonstrated that micro-nano bubbles improved the shearing ability of airflow, leading to better atomization and reduced axial penetration length. Furthermore, the benefits of micro-nano bubble fuel mixtures were more pronounced at lower injection pressures, making them particularly suitable for optimizing combustion in engines with lower compression ratios. These findings further reinforce the potential of nanobubbles in enhancing fuel distribution and improving combustion efficiency.

Effervescent spray, a two-phase flow where gas bubbles are injected along with the liquid to create a small mean droplet diameter, has also been a motivation for this study as they are already in use in turbines and industrial burners. However, the spray atomization in effervescent systems is often non-uniform, requiring the design of specialized atomizers to achieve optimal performance [24,25]. Introducing gas as nanobubbles into the liquid provides an alternative approach to mimic the effervescent spray effect, potentially improving atomization uniformity and eliminating the need for complex atomizer designs. This approach could enable the use of a mono-fuel system rather than two separate flows in an injection, simplifying the fuel delivery process while enhancing spray characteristics.

Despite the promising results of nanobubble-enhanced fuels, their influence on GDI sprays has not been extensively studied. Given that spray characteristics play a critical role in combustion efficiency, understanding the impact of air nanobubbles (ANBs) on fuel atomization is essential. This study aims to investigate the generation of ANBs in gasoline using a hydrodynamic cavitation method and their subsequent influence on spray properties in GDI systems. Specifically, this research seeks to:

1. Develop a stable method for producing air nanobubbles in gasoline using a custom-designed nanobubble generator.
2. Characterize the size distribution, concentration, and zeta potential of nanobubbles in gasoline using dynamic light scattering (DLS).
3. Analyze the impact of ANBs on spray characteristics, including penetration length, cone angle, droplet size and axial velocity in a constant volume chamber.

Table 1
Fuel properties.

Parameter	Value
Stoichiometric air/fuel ratio	14.7
Density (kg/m^3) @ 298 K	730
Kinematic viscosity (mm^2/s) @ 313 K	0.6
Boiling point (K)	230
Surface tension (mN/m) @ 293 K	21.5
Research octane number	95
Lower calorific value (MJ/kg) @ 298 K	44.2

By addressing these objectives, this study aims to provide new insights into the role of nanobubbles in fuel injection and atomization processes. The findings could contribute to the advancement of cleaner and more efficient combustion technologies, paving the way for next-generation fuel formulations.

2. Methodology

2.1. Nanobubble generation

The generation of air nanobubbles in liquid fuel (standard gasoline-E10 95 RON-Regular Unleaded) is achieved through hydrodynamic cavitation using a custom-designed nanobubble generator. The fuel properties are listed in Table 1. The generation system operates in a fully closed-loop configuration, as illustrated in Fig. 1, in which gasoline is continuously circulated from Tank 1 through a pump. Air is passively entrained at the pump inlet via a flow meter, enabling precise control of the air intake rate. The rapid pressure drop at the pump inlet, combined with high shear and vortex-induced cavitation within the flow, promotes the breakup of entrained air into micro- and nanobubbles. The resulting nanobubble-enriched fuel is discharged into Tank 2 and subsequently recirculated within the closed loop until the desired nanobubble concentration is achieved. Pressure relief valves installed on the tanks, along with a fume-capturing unit, ensure safe and stable operation of the system. The primary advantages of this method include the bulk production and the ability to produce a high concentration of nanobubbles with a uniform size distribution. Despite the diversity in these techniques, the underlying physics of bubble formation involves the reduction of pressure facilitated by surface tension and energy deposition [26,27]. Further details on nanobubble generation based on the principles of hydrodynamic cavitation are well documented in the literature [1,9,28].

During the NBs generation process, the airflow rate was maintained at a constant rate of 1.5 LPM, while the fuel flow rate was dynamically adjusted to sustain this suction. The fuel was continuously recirculated between the high-pressure and low-pressure tanks in a closed-loop system. This circulation was maintained until the desired concentration exceeded 10^{11} bubbles/ml.

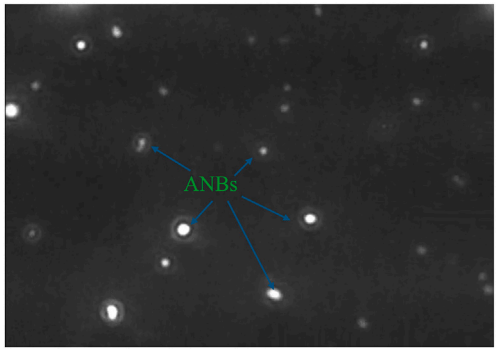

Fig. 2. Light scattered from ANBs captured using nanoparticle tracking analysis (NTA) with a Malvern NanoSight instrument, confirming their presence in the sample.

2.2. Characterization of nanobubbles

Dynamic light scattering technique (DLS) -based system is utilised for the nanobubble characterization. Dynamic light scattering relies on analyzing how the autocorrelation function of scattered light intensity changes over time. Smaller bubbles cause the scattered light intensity to decorrelate more quickly than larger bubbles, making it possible to determine their size based on this difference [6]. Malvern Panalytical offers the ZetaSizer Ultra, an instrument designed to analyze bubbles ranging from 3 nm to 10 μm. It performs dynamic light scattering (DLS) measurements from three angles: front scatter, side scatter, and back scatter. The system then provides average results for particle size and concentration. Additionally, Nanoparticle Tracking Analysis (NTA) measurements, as shown in Fig. 2, confirm the presence of ANB in the sample.

The instruments provide data on particle size distribution and total particle concentration, which are then used to calculate additional parameters such as the gas pressure inside the bubbles, the gas density in the nanobubbles, and with them the volume and mass of air dissolved in the fuel as nanobubbles. To calculate the internal gas pressure within the nanobubbles, the Young-Laplace Eq. (1) is applied [19,29].

$$P_i = P_a + \frac{4ST}{D} \tag{1}$$

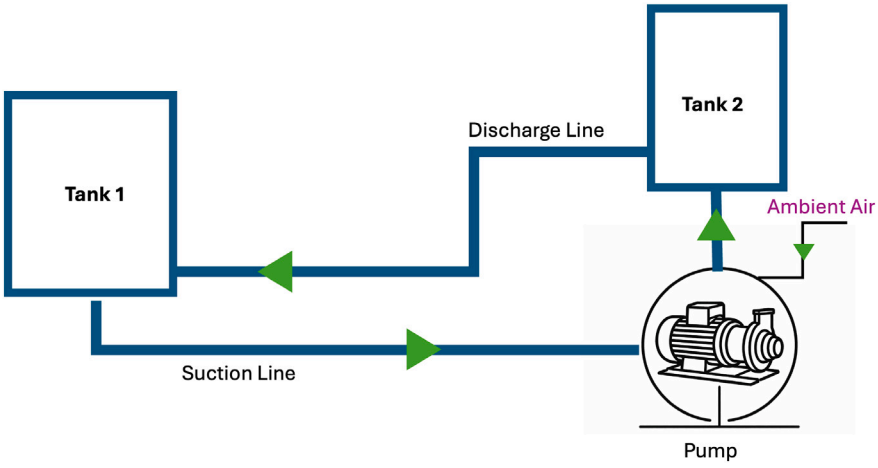

Fig. 1. Schematic of nanobubble generation setup.

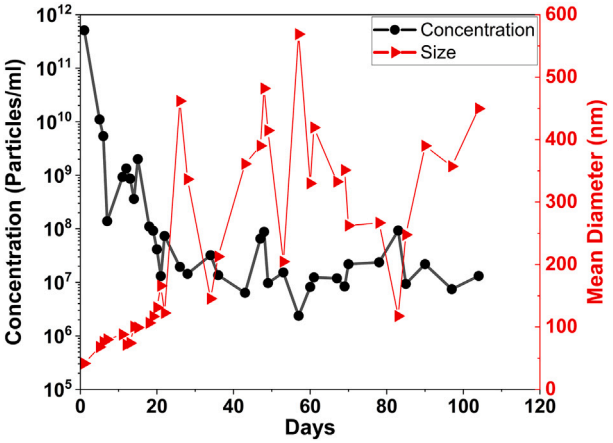

Fig. 3. Particle characterization: nonburnable concentration and mean diameter (size) vatiation over time.

Here Pi is the internal pressure, Pa is the ambient pressure, ST is the surface tension of the fuel and D is considered as the mean diameter of the particle size distribution obtained from the ZetaSizer Ultra. Input values in the instrument are ST and the refractive index (1.41) of gasoline.

2.3. ANB long term stability in gasoline

The concentration and mean diameter of air nanobubbles (ANBs) in gasoline were monitored over time to evaluate their stability and dispersion behavior. Fig. 3 presents the variation of nanobubble concentration and mean diameter over a period of 100 days. Immediately after production, the nanobubble concentration was measured at $5.12X10^{11}$ particles/mL, which was the average of three samples. The mean diameter of the distribution at this stage was approximately between 35–50 nm. This initial high concentration is noteworthy, as similar levels have not been widely reported in previous literature. However, the concentration showed a gradual decline over time, a trend consistent with findings from previous studies [19,20]. After one week, the nanobubble concentration decreased significantly to around 10^8 particles/mL, aligning with previously observed trends in nanobubble research [19,23]. By the third week, the concentration further stabilized at 10^7 particles/mL, where it remained relatively constant with only minor fluctuations over the rest of the observation period, such long term behavior is also noted in literature for air NBs in DI water [30,31]. This trend suggests that nanobubbles experience an initial phase of nucleation and stabilization, followed by coalescence and dissolution over time. The mean diameter exhibits significant fluctuations, varying between 50 nm to 500 nm, with larger bubbles appearing intermittently, possibly due to bubble coalescence.

At the initial stages, when the mean nanobubble (NB) diameter was below 100 nm, the zeta potential was measured at approximately −30 mV. As the NB size increased to the range of 200–400 nm, the zeta potential decreased to between −12 mV and −18 mV, consistent with the findings of Ahmed et al. [32], who reported that smaller NBs exhibit more negative zeta potentials than larger ones. This behavior is in stark contrast to pure gasoline, which typically exhibits a positive zeta potential ranging from +5 mV to +7 mV. Such negative zeta potential values have been widely observed for various gases dispersed in deionized water, with values exceeding −40 mV being reported. Notably, a zeta potential below −20 mV is generally considered an indicator of colloidal stability [33].

2.4. Spray characterization

Once the ANB fuel was generated, a constant volume chamber was used to investigate the impact of nanobubbles on spray behavior. A single-hole gasoline direct injection (GDI) injector was employed for the spray study. Three injection pressures were tested: 50 bar, 100 bar, and 150 bar.

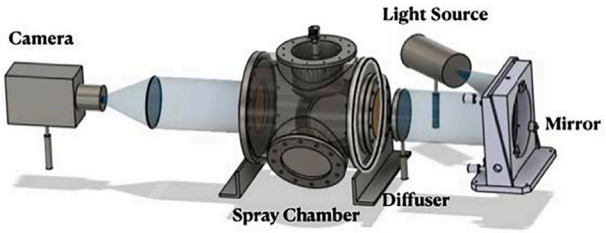

Fig. 4. Diffused Back Illumination (DBI) setup.

Table 2
Experimental and optical settings for diffused backlight imaging (DBI).

Parameter	Specification
Injection system	Single-hole GDI injector
Injection pressure	50, 100, 150 bar
Injection duration	3 ms
Fuel	Gasoline (baseline) and ANB-enriched gasoline
Chamber pressure	1 bar (ambient)
Chamber temperature	~23 °C
Illumination method	Diffused backlight (white light)
High-speed camera	Photron NOVA S12
Frame rate	20,000 fps
Exposure time	15.3 μs
Image resolution	1024 × 896 pixels

Diffused Backlight Imaging (DBI) was employed to visualize the liquid phase of the spray. In the DBI configuration, the chamber was illuminated using a uniform back-illumination light source, and the spray-induced light attenuation was recorded using a high-speed camera. A high-stability LED light source (Innovative Scientific Solutions Inc., ISSI), operating at a wavelength of 460 nm, was used to provide back-illumination. The LED module was operated in continuous (DC) mode to ensure uniform and temporally stable illumination during image acquisition. A schematic of the DBI setup is shown in Fig. 4, and the corresponding high-speed camera settings are summarized in Table 2.

The collected images were analyzed to determine key spray parameters such as penetration length, cone angle, and near-nozzle cavitation effects. The results were compared with baseline gasoline to evaluate the influence of nanobubbles on spray atomization.

2.5. Image processing

Fig. 5 summarizes the different stages of the image processing procedure using MATLAB in this study. First, the captured images were converted to grayscale and processed using background subtraction to isolate the spray-induced light attenuation. Second, appropriate thresholds were set to remove image noise and extract the spray boundary. Afterward, the results of macroscopic spray characteristics were obtained through calculation.

To analyze the macroscopic spray characteristics, key parameters were introduced to quantify spray morphology. One such parameter is the Spray Density Factor (SDF). The Spray Density Factor (SDF) is a non-dimensional metric used to quantify the relative optical density of a spray plume based on the intensity distribution of background-subtracted DBI images. SDF reflects the degree of light attenuation caused by the liquid phase within the detected spray region.

$$SDF = \frac{\sum_{i=1}^{n} I_i}{n \cdot I_{\max}} \quad (2)$$

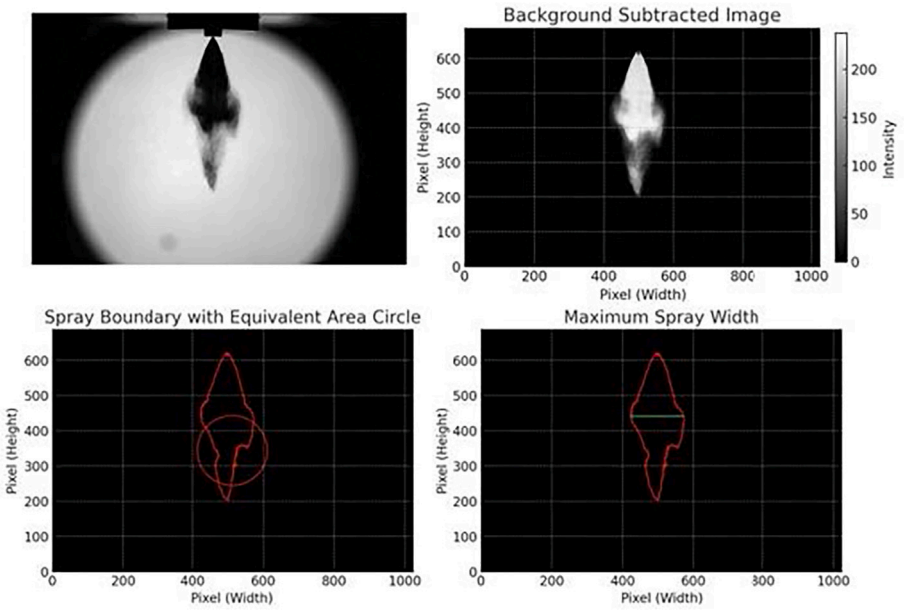

Fig. 5. Image processing steps.

Where in Eq. (2), I_i represents the background-subtracted grayscale intensity of the ith pixel within the detected spray region, where higher intensity corresponds to stronger light attenuation by the liquid phase. Here, n is the total number of detected spray pixels and I_{max} denotes the maximum background-subtracted pixel intensity within the spray region, used for normalization.

The Spray Density Factor (SDF) provides a measure of the relative optical density of the liquid spray based on background-subtracted DBI images. Since the image processing removes the background illumination, higher pixel intensities correspond to stronger light attenuation by the liquid phase and thus higher local liquid-phase concentration. Accordingly, higher SDF values indicate optically denser spray regions, where the liquid phase is more concentrated and compact. In contrast, lower SDF values correspond to optically dilute and spatially dispersed spray structures, which may arise from enhanced spray breakup and dispersion. It is important to note that SDF does not directly represent spray uniformity or air–fuel mixing; rather, it reflects the distribution of liquid-phase optical density within the detected spray region. Therefore, SDF should be interpreted in conjunction with other macroscopic spray parameters (e.g., penetration length and spray area) and droplet-scale measurements to assess spray atomization behavior.

Fig. 6 illustrates an example of spray visualization using SDF, where the left image shows the spray boundary detection, and the right image represents the intensity distribution.

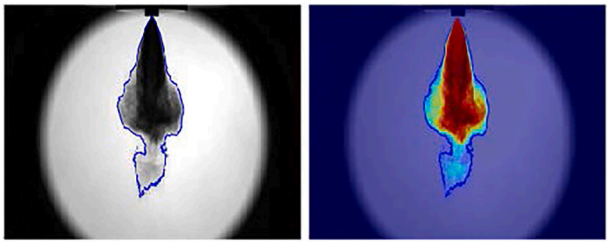

Fig. 6. Spray density factor (SDF) visualization showing spray boundary detection (left) and intensity distribution (right).

2.6. PDPA experiment setup

The spray droplet size distribution and droplet velocity were analyzed using a PDPA system, supplied by Dantec Dynamics. The experiments were conducted in a constant volume chamber maintained at ambient pressure and a controlled room temperature of approximately 23°C and nitrogen gas at 1 bar of constant pressure was supplied to remove the injected fuel and maintain optically transparent vision for measurement. The PDPA system and laser specifications are provided in Table 3.

Table 3
Experimental and optical settings for phase doppler anemometry (PDA).

Parameter	Specification
PDA supplier	Dantec Dynamics
Injection system	Single-hole GDI injector
Injection pressure	150 bar
Fuel	Gasoline (baseline) and ANB-enriched gasoline
Measurement distances	30, 40, 50 mm below injector tip
Chamber pressure	1 bar
Chamber temperature	~23 °C
Probe diameter	60 mm
Laser type	DPSS Argon-Ion laser
Laser wavelength	532 nm
Focal length	310 mm
Beam diameter	2.2 mm
Beam expansion ratio	1.9
Power output	400 mW
Modulation frequency	40 MHz
Scattering angle	70°
Spatial resolution	2 mm grid spacing
Samples per location	10,000 droplets

The measured parameters included the individual droplet diameter (Di) and axial velocity (Vi) at the probe volume location, which were subsequently used to calculate the Sauter Mean Diameter (SMD or D32) and the mean axial velocity (Vm). For spatial analysis, measurements were taken at three planes located 30 mm, 40 mm, and 50 mm downstream from the injector tip at an injection pressure of 150 bar. The PDA measurement locations were selected to represent distinct stages of spray development while ensuring reliable optical access and sufficient droplet statistics. The location at 30 mm represents the near-nozzle

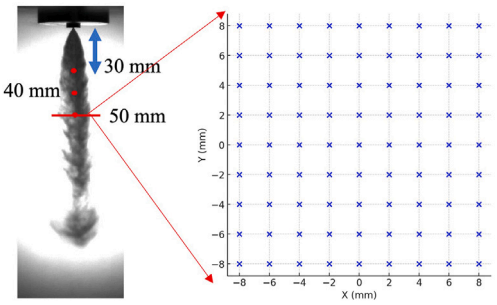

Fig. 7. Measurement planes and spatial grid for droplet characterization downstream of the injector.

region, where droplets are freshly formed following primary breakup and the spray remains relatively dense. This region is strongly influenced by injector exit conditions and early atomization mechanisms. The 40 mm location corresponds to the intermediate spray region, where secondary breakup, droplet interaction, and momentum exchange with the surrounding gas become more pronounced. The far-field region at 50 mm represents a more developed spray, where droplet dispersion, coalescence, and aerodynamic deceleration dominate the spray dynamics. These locations were chosen to balance physical relevance and measurement reliability. Closer axial positions ($< 30\ mm$) were avoided due to excessive spray density and multiple scattering effects, which can compromise PDA signal quality. Positions beyond 50 mm exhibited reduced droplet count and increased intermittency, leading to less robust statistics. The selected locations therefore provide a consistent and representative characterization of spray evolution while maintaining reliable PDA measurements. Within each plane, a measurement matrix was established, spanning from -8 mm to $+8$ mm with a 2 mm mesh grid resolution, resulting in 81 measurement points per plane, as illustrated in Fig. 7. To ensure statistical reliability, 10,000 droplet data points were sampled and processed at each measurement location.

2.7. PDPA data processing

Contour plots illustrating the SMD and droplet velocity were created for three planes positioned 30 mm, 40 mm, and 50 mm below the injector tip. Additionally, an axial plot was generated by extracting data along the x-axis (at $Y = 0$) from each plane to analyze the spray characteristics along the central line of the injector tip, extending 8 mm from the center on both sides. To ensure a systematic analysis, the spray was divided into three distinct zones:

- **Zone 1:** The initial phase of the injection or needle lift zone.
- **Zone 2:** The main spray event or needle hold phase.
- **Zone 3:** The tail portion of the injection.

For a fair comparison, Zone 1 was selected for post-processing due to its consistent droplet distribution. In Zones 2 and 3, the spray behavior varies significantly depending on the probe volume's position relative to the laser direction. Due to the dense nature of the spray, droplet detection in Zone 2 is sometimes obstructed, leading to missing data points and potential bias in overall trends. In Zone 3, as the spray disperses further, the number of detected droplets decreases progressively, making the region less reliable for direct comparison. At 50 mm below the nozzle, the tail zone (Zone 3) becomes almost negligible, as illustrated in Fig. 8, which presents the droplet velocity scatter plot. Thus, while an ideal comparison would involve analyzing each zone separately, Zone 1 was chosen to ensure consistency and minimize bias across different measurement locations.

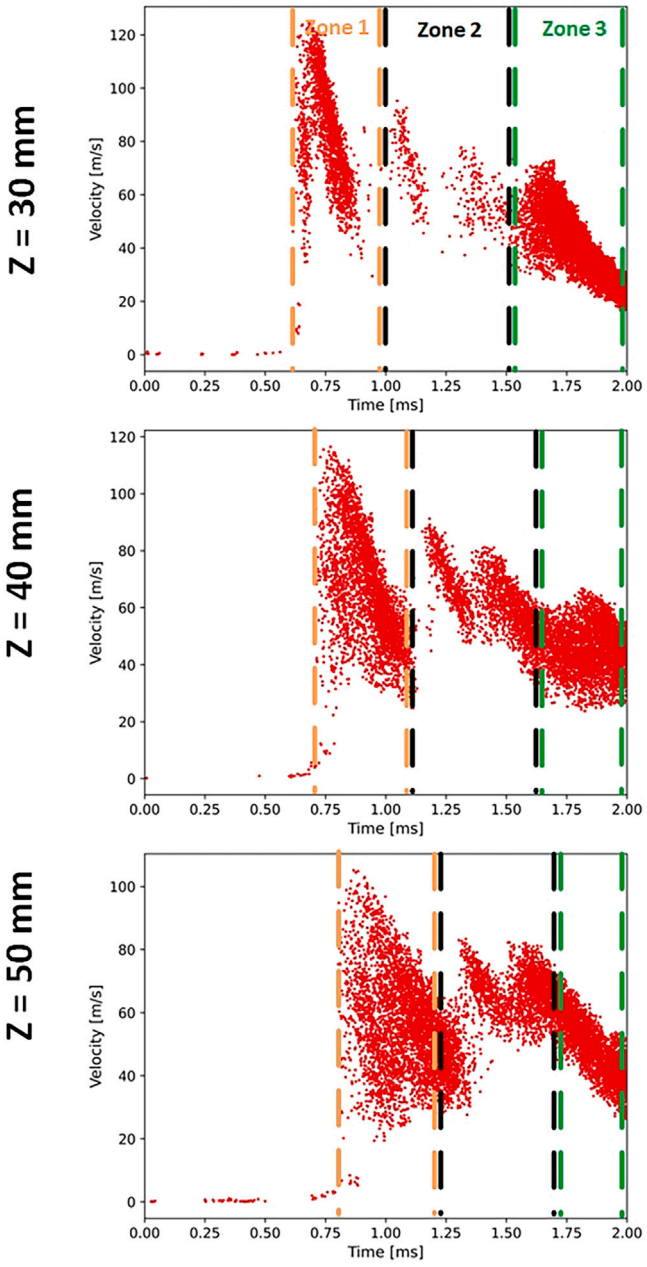

Fig. 8. Droplet velocity distribution in different plane.

3. Results and discussion

3.1. Spray characterization

To investigate the effect of air nanobubbles (ANBs) on spray behavior, a temporal evolution of spray morphology analysis was conducted at an injection pressure of 150 bar, 100 bar and 50 bar injection pressure for both baseline gasoline and ANB fuel. Fig. 9 presents the evolution of spray at an injection pressure of 150 bar, comparing baseline gasoline (top row) and air nanobubble (ANB) fuel (bottom row) at different time intervals. At the early stages of injection (0.4 ms), both baseline gasoline and ANB fuel show no visible spray structure, indicating that the fuel has just started penetrating the chamber. This phase primarily represents the injection delay, during which the fuel travels from the injector nozzle before forming a well-defined spray. By 0.75 ms, the spray becomes visible, with both fuels exhibiting a well-defined liquid column emerging from the injector nozzle. As the injection progresses

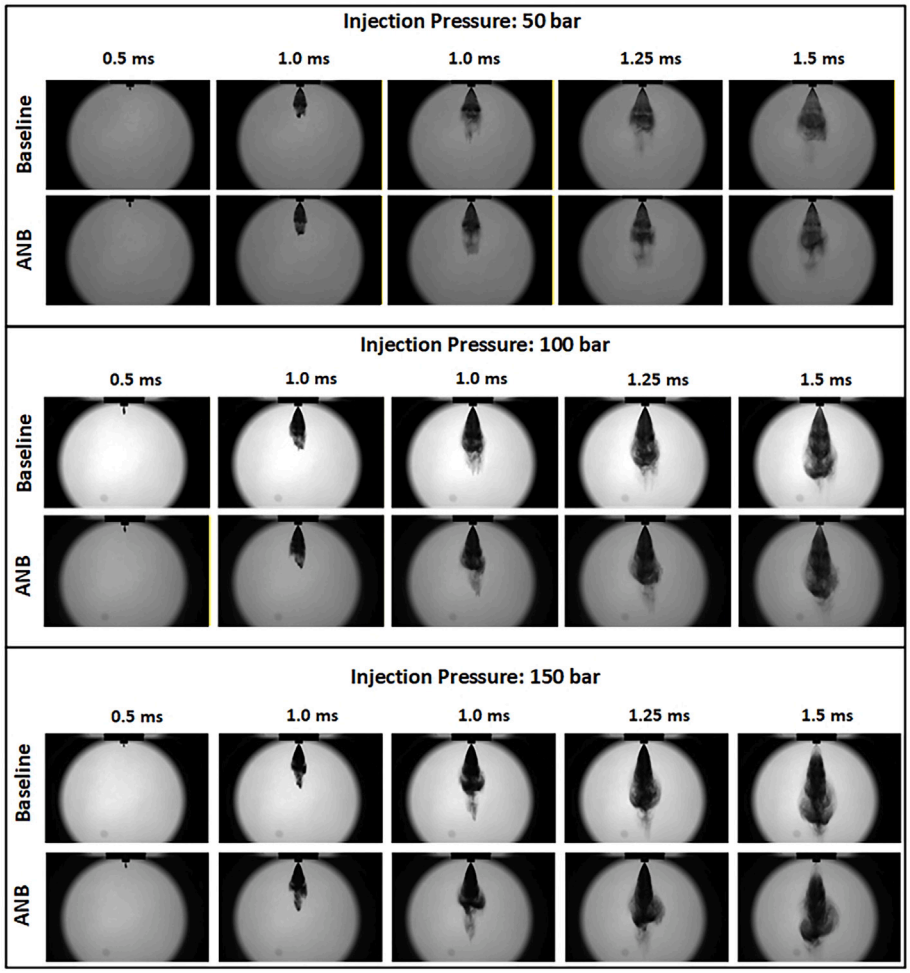

Fig. 9. Temporal evolution of spray morphology of baseline gasoline and ANB fuel at different injection pressure.

(1.0 ms - 1.25 ms), the ANB fuel spray appears to have a wider spray width at the bottom and more dispersed droplets compared to baseline gasoline. The baseline gasoline spray maintains a more concentrated liquid phase, with larger fuel clusters visible at the edges. The irregularities in the ANB fuel spray boundary indicate an increase in turbulent structures and cavitation-induced breakup, which may enhance fuel vaporization. To quantify the differences observed in spray evolution, the following section will provide a detailed analysis of spray penetration length and cone angle.

Fig. 10 shows the penetration length evolution of baseline gasoline and ANB fuel at three different injection pressures. All test conditions were repeated ten times, and the average values of the results are reported. At all tested injection pressures, ANB fuel exhibits a shorter penetration length than baseline gasoline. The difference in penetration length becomes more pronounced at higher injection pressures, particularly at 150 bar, where the deviation is most significant. The initial penetration rates for both fuels are similar, but as the spray develops, ANB fuel shows a slightly slower penetration growth. The presence of air nanobubbles within the liquid fuel can promote localized micro-scale instabilities during injection. Under the high shear and pressure gradients associated with GDI injection, nanobubbles may undergo rapid expansion and collapse, generating localized disturbances within the liquid jet. These micro-explosion–like events can enhance droplet breakup, leading to the formation of finer droplets with reduced axial momentum [34,35] As a result, the ANB-enriched fuel exhibits lower penetration lengths compared to baseline gasoline [23].

The cone angle was measured for a fully developed spray after 1 ms. The reported values were calculated between 1 ms and 1.8 ms after SOI, as the spray plume evolved properly by this time, ensuring enough spray boundary points for accurate measurement. The cone angle was determined by selecting the first 100 points on both sides of the spray boundary. A straight line was fitted to these points, and the overall spray cone angle was obtained from the slope of these two inclined lines.

Fig. 11 depicts the evolution of the overall spray cone angle for the tested fuels at different injection pressures. At 50 bar injection pressure, baseline gasoline exhibits relatively larger temporal fluctuations in cone angle compared to the ANB-enriched fuel, which shows a more stable and slightly reduced cone angle. As the injection pressure increases to 100 bar, both fuels exhibit similar cone angle trends, although the ANB fuel continues to display marginally reduced fluctuations, indicating a more stable spray boundary. At 150 bar, the cone angle values for both fuels converge and remain nearly identical, suggesting that at higher injection pressures the spray development is predominantly governed by injection momentum, thereby reducing the influence of fuel formulation on macroscopic spray geometry. At lower injection pressures (50 bar and 100 bar), the presence of nanobubbles may influence the near-nozzle spray development. Furthermore, near the injector tip, the spray remains relatively compact due to the dominance of axial momentum. However, as the spray evolves downstream, the enhanced breakup and momentum dissipation associated with nanobubble-induced instabilities lead to increased radial dispersion. This behavior is reflected by the larger spray area observed at downstream locations for ANB fuel, indicating

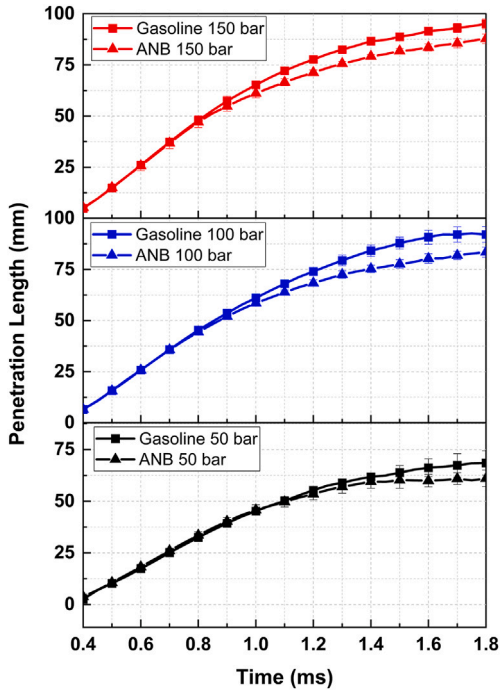

Fig. 10. Liquid penetration length for gasoline and ANB + gasoline.

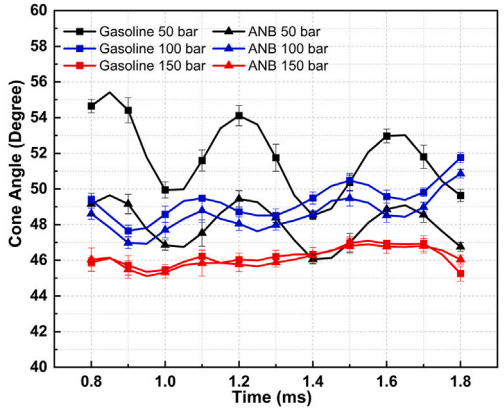

Fig. 11. Spray cone angle for gasoline and ANB + gasoline.

improved spatial distribution of the liquid phase despite reduced penetration. However, it should be emphasized that spray cone angle alone is not a direct indicator of atomization quality. In the present study, the cone angle trends are therefore interpreted in conjunction with penetration length, spray area, SDF, and droplet-scale PDA measurements to assess overall spray breakup and dispersion behavior.

Fig. 12 shows the comparison of the Spray Density Factor (SDF) for baseline gasoline and ANB-enriched fuel at different injection pressures. Compared to baseline gasoline, the ANB fuel exhibits lower SDF values, particularly at higher injection pressures (100 bar and 150 bar), indicating a reduction in optical spray density. This behavior suggests enhanced spray dispersion and a more spatially distributed liquid phase for the ANB-enriched fuel. Baseline gasoline exhibits relatively higher SDF values, corresponding to a more optically dense and compact spray structure. In contrast, the reduced SDF observed for ANB fuel indicating enhanced secondary breakup and dispersion. These results indicate that the presence of nanobubbles modifies the spray momentum distribution and breakup behavior during injection. While the enhanced dispersion may be associated with localized instabilities introduced by entrained

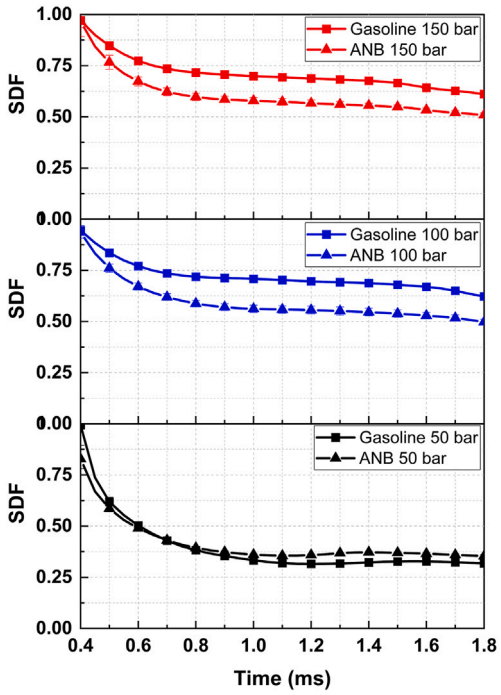

Fig. 12. Spray density factor of gasoline and ANB + gasoline at different injection pressure.

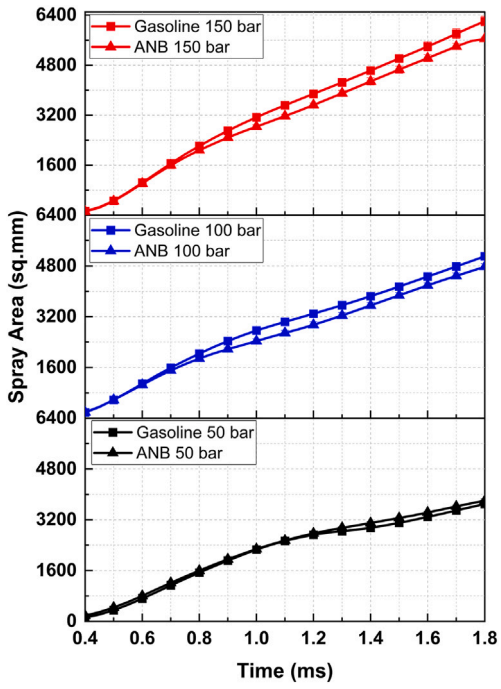

Fig. 13. Temporal evolution of the projected spray area for baseline gasoline and ANB + gasoline fuel at injection pressures of 50, 100, and 150 bar.

nanobubbles, detailed internal nozzle flow diagnostics are required to conclusively identify the underlying mechanisms. It should be noted that SDF represents relative optical spray density rather than air–fuel mixing directly, and its interpretation should be considered together with other macroscopic and droplet-scale spray parameters.

Fig. 13 shows the temporal evolution of the projected spray area for baseline gasoline and ANB-enriched fuel at injection pressures of

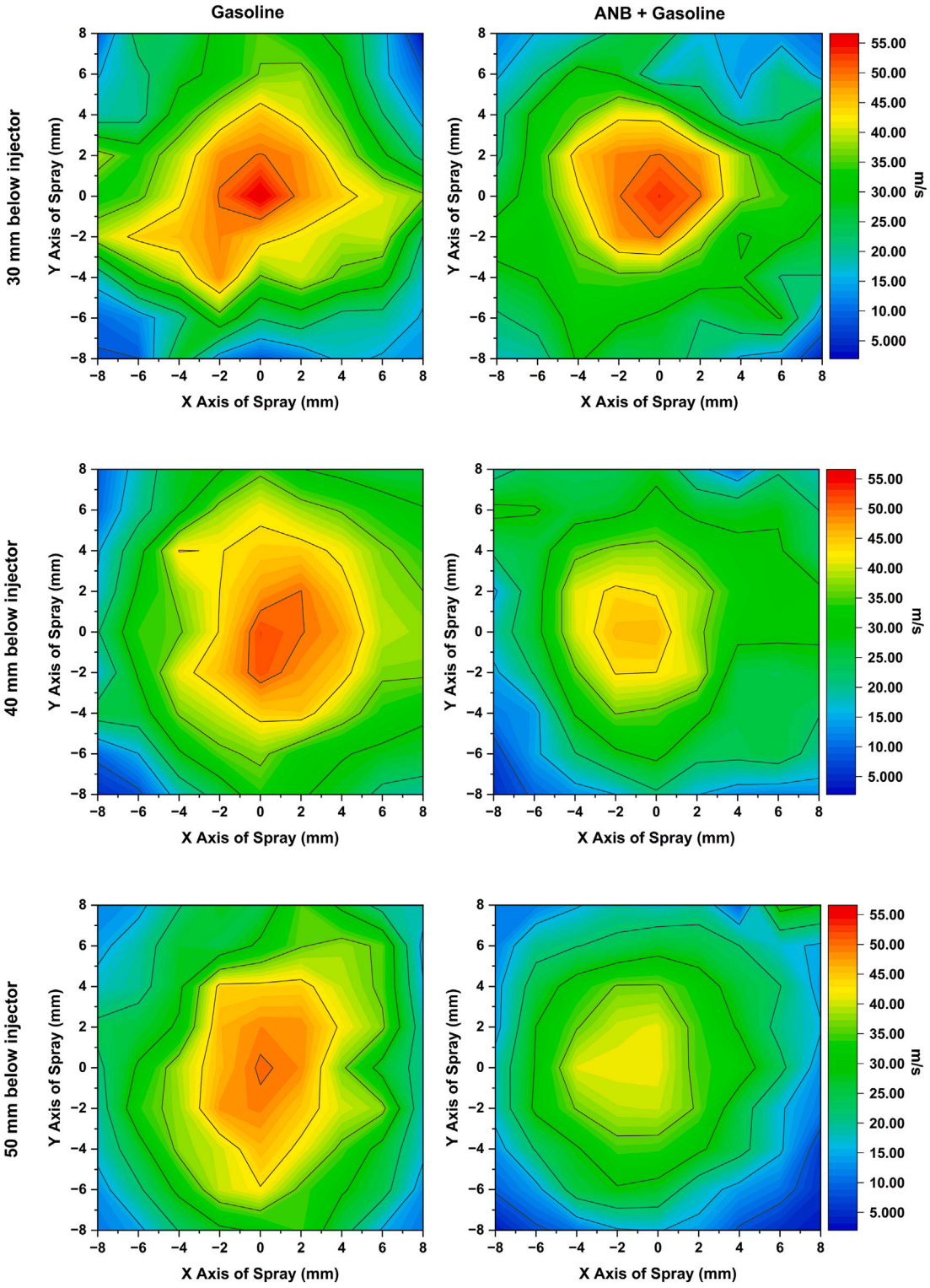

Fig. 14. Contour plot for droplet velocity distribution.

50, 100, and 150 bar. For all cases, the spray area increases with time after the start of injection as the liquid jet develops and spreads. At 100 bar and 150 bar injection pressures, baseline gasoline exhibits a slightly larger projected spray area compared to the ANB-enriched fuel throughout the spray evolution. This behavior is attributed to the higher axial momentum of the baseline fuel, which promotes stronger geometric spreading of the spray plume. Although clear differences are observed in spray penetration length and cone angle between the two fuels, the projected spray area remains broadly comparable across most operating conditions. This behavior can be explained by the different spatial evolution of the spray. While the ANB-enriched fuel exhibits a relatively narrower and more stable spray structure in the near-nozzle

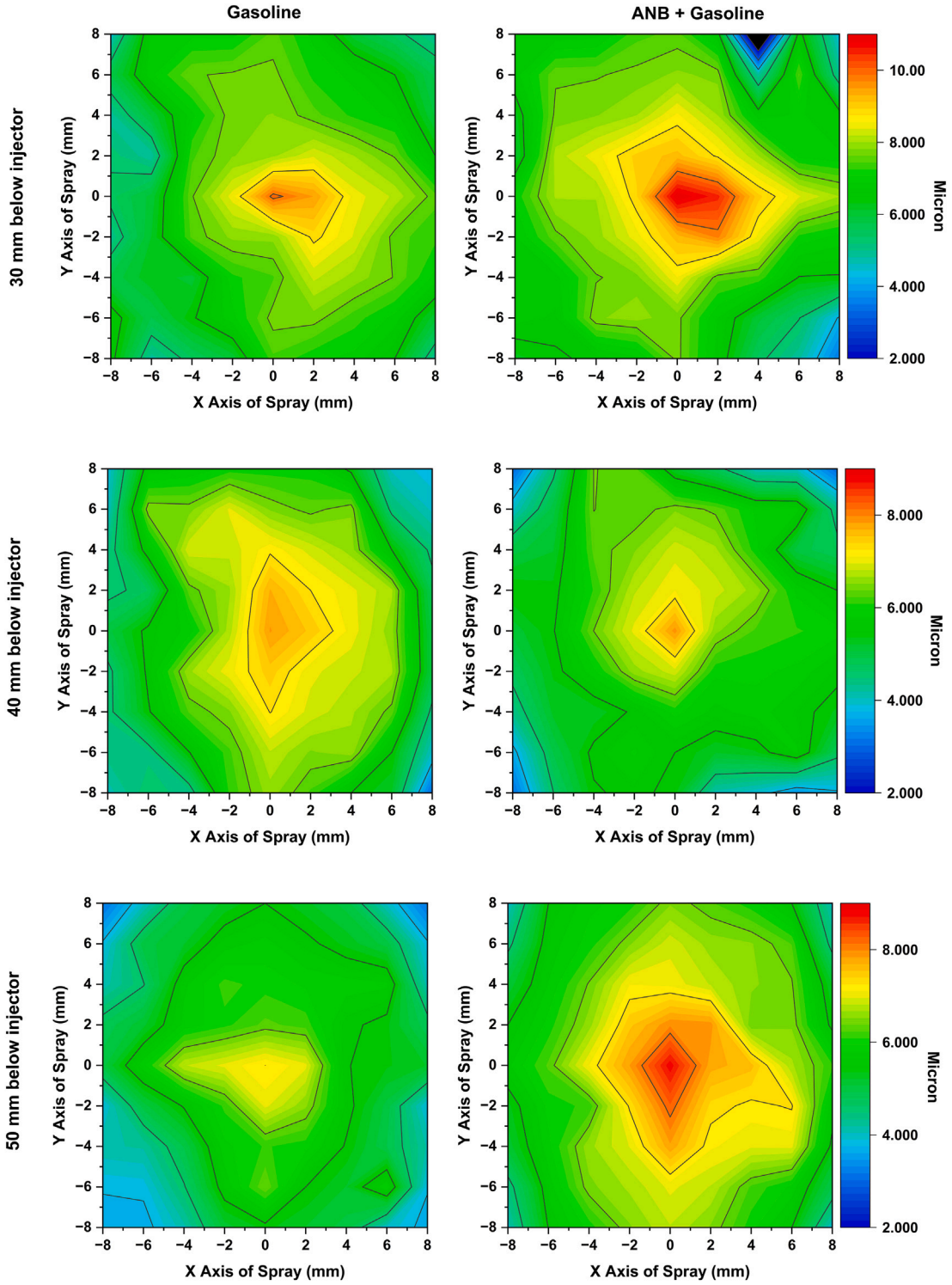

Fig. 15. Contour plot for SMD (D32) distribution.

region, enhanced breakup and momentum dissipation associated with nanobubble-induced micro-scale instabilities promote increased radial dispersion in the downstream region. As a result, the initially narrower spray of the ANB fuel expands later in the spray development, leading to a spray area comparable to that of baseline gasoline despite reduced penetration and cone angle. When interpreted together with the Spray Density Factor (SDF) and PDA measurements, the reduced spray area for ANB fuel does not indicate inferior dispersion. Instead, the lower SDF and reduced droplet axial velocities suggest enhanced breakup and faster momentum dissipation, resulting in a more optically dilute and finely dispersed spray.

3.2. Droplet characterization

To investigate the influence of air nanobubbles (ANB) on droplet size and velocity, experiments were conducted at an injection pressure of 150 bar. Measurements were recorded at three axial locations—30 mm, 40 mm, and 50 mm below the injector tip—captured as contour plots in Figs. 14 and 15. These plots illustrate the spatial distribution of droplet

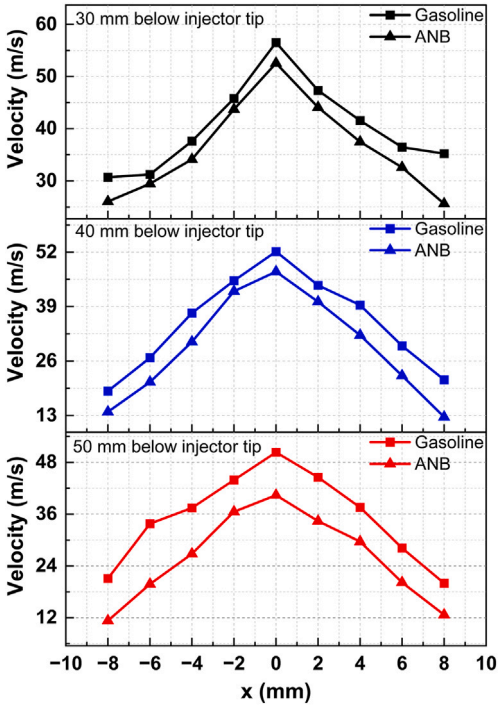

Fig. 16. Axial plot of droplet velocity.

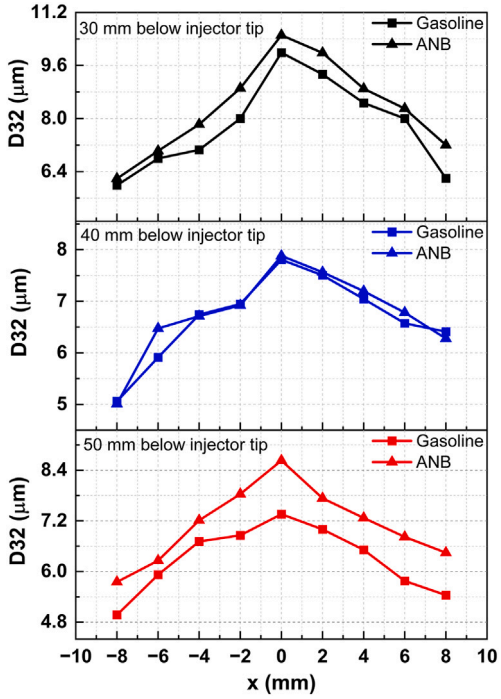

Fig. 17. Axial plot of SMD (D32).

velocity and size (D32) for both baseline gasoline and ANB + Gasoline mixtures. The D32 contour plots (Fig. 15) indicate that the baseline gasoline spray exhibits a concentrated region of larger droplets, especially at 30 mm, whereas the ANB + Gasoline mixture demonstrates a more uniform size distribution across the spray field. This uniformity persists with increasing distance from the injector, suggesting that ANB promotes stable droplet formation. Furthermore, the velocity contour plots (Fig. 14) reveal a significant reduction in droplet velocity for the ANB + Gasoline mixture, particularly in the central region. This reduction can be attributed to enhanced droplet breakup caused by the presence of nanobubbles, which promote secondary atomization and reduce the average droplet size. Such behavior contrasts with the baseline gasoline, where higher velocities and non-uniform droplet distribution are evident. However, due to the reduced velocity, the smaller droplets coalesce and increase the droplet size at 50 mm below the injector tip, as shown in Fig. 15. This further enhances aerodynamic drag and subsequently reduces droplet velocity. The introduction of ANB effectively minimizes the characteristic uneven distribution typically observed in effervescent sprays, highlighting its potential to enhance spray homogeneity and improve atomization characteristics. Additionally, axial profiles for both baseline gasoline and ANB + Gasoline, extending from the spray center to the lateral boundaries, are presented in Figs. 16 and 17, further illustrating the effect of ANB on spray dynamics.

The droplet velocity is consistently lower for the ANB + Gasoline mixture compared to baseline gasoline, a trend that aligns with the shorter spray penetration length observed in the previous section. At 30 mm below the injector tip in the central region, the droplet velocity decreases from 57.23 m/s for gasoline to 52.67 m/s for ANB + Gasoline, representing a reduction of approximately 7.97%. Currently, the droplet size (D32) in this region shows a slight increase from 9.98 μm for gasoline to 10.51 μm for ANB + Gasoline, corresponding to a 5.04% increase.

These observations suggest that the introduction of nanobubbles leads to an increase in droplet diameter potentially due to enhanced coalescence, which further enhances the aerodynamic drag and subsequently reduces droplet velocity [36].

At 40 mm below the injector (Fig. 17), the D32 values for gasoline and ANB + gasoline are nearly identical, measuring 7.49 μm and 7.55 μm, respectively. This minimal variation indicates a high potential for droplet collision and coalescence, which likely contributes to the further increase in droplet diameter observed at 50 mm below the injector, where the D32 for ANB + Gasoline exceeds 8 μm. This behavior may be attributed to the interaction between droplets in the spray, which leads to coalescence and growth. However, a more comprehensive analysis is necessary to fully understand these phenomena, as the limited available literature on nanobubble-enhanced sprays complicates the identification of the underlying mechanisms. Furthermore, it is important to note that the results presented here are focused solely on Zone 1 (as per Fig. 8), with the characterization of the spray needle lift phase, while the tail and needle hold zone are not discussed in this study.

4. Conclusions

This study investigated the impact of air nanobubbles (ANBs) on gasoline direct injection (GDI) spray characteristics, focusing on penetration length, spray cone angle, droplet size and axial velocity at three injection pressures (50 bar, 100 bar, and 150 bar). A custom-built nanobubble generator using hydrodynamic cavitation was employed to produce ANB fuel, and high-speed imaging and PDA techniques were used to analyze the spray behavior in a constant volume chamber. The key findings from the results are listed below:

- High concentrations of stable air nanobubbles were successfully generated in gasoline.
- Long-term stability of nanobubbles in gasoline was confirmed for up to 120 days, with a consistently negative zeta potential in the range of −20 to −25 mV, indicating electrostatic stability.
- The results demonstrate that the addition of air nanobubbles has a significant influence on spray evolution.
- Compared to baseline gasoline, ANB-enriched fuel exhibited a reduction in spray penetration of approximately 7 to 13% across the investigated injection pressures, indicating a significant modification of spray evolution.
- PDA measurements showed that the introduction of nanobubbles resulted in a 7.97% reduction in droplet axial velocity and a 5.04%

increase in mean droplet size at 30 mm downstream of the injector tip, indicating enhanced aerodynamic resistance and intensified spray–gas interaction. At 40 mm, the droplet size exhibited minimal variation between fuels, suggesting that droplet interactions such as collision and coalescence may become more pronounced as the spray evolves downstream.

These results demonstrate that air nanobubbles significantly influence spray breakup dynamics, leading to enhanced atomization, improved spray stability, and better air–fuel mixing. The findings highlight the potential of nanobubble-enhanced fuels for optimizing GDI spray behavior. Future work will focus on detailed near-nozzle spray analysis, with particular emphasis on secondary breakup mechanisms, as well as quantifying combustion and emissions performance. The applicability of this approach to non-fossil fuels and the use of hydrogen nanobubbles in liquid fuels will also be explored.

CRediT authorship contribution statement

Abinash Biswal: Writing – original draft, Methodology, Formal analysis, Data curation, Conceptualization. **Suraj Prashad Sharma:** Writing – original draft, Formal analysis, Data curation. **Roger Cracknell:** Conceptualization. **Hua Zhao:** Writing – review & editing, Supervision, Conceptualization. **Xinyan Wang:** Writing – review & editing, Supervision, Funding acquisition, Conceptualization.

Declaration of competing interest

The authors declare that they have no known competing financial interests or personal relationships that could have appeared to influence the work reported in this paper.

Acknowledgments

This work was supported by a UKRI Future Leaders Fellowship (MR/ T042915/1, UKRI1057). The authors also gratefully acknowledge the support of Malvern Panalytical for assistance in characterizing the nanobubbles, as well as the valuable technical support provided by Andrew Selway and Eamon Wyse.

Data availability

Data will be made available on request.

References

[1] Favvas EP, Kyzas GZ, Efthimiadou EK, Mitropoulos AC. Bulk nanobubbles, generation methods and potential applications. Curr Opin Colloid Interface Sci Aug 2021. https://doi.org/10.1016/j.cocis.2021.101455
[2] Patel AK, Singhania RR, Chen CW, Tseng YS, Kuo CH, Wu CH, Di Dong C. Advances in micro- and nano bubbles technology for application in biochemical processes. Environ Technol Innov Aug 2021;23. https://doi.org/10.1016/j.eti.2021.101729
[3] Wang Y, Wang T. Preparation method and application of nanobubbles: a review. Coatings 9, 2023. https://doi.org/10.3390/coatings13091510
[4] Phan KKT, Truong T, Wang Y, Bhandari B. Nanobubbles: fundamental characteristics and applications in food processing. Trends Food Sci Technol Jan 2020. https://doi.org/10.1016/j.tifs.2019.11.019
[5] Wang X, Li P, Ning R, Ratul R, Zhang X, Ma J. Mechanisms on stability of bulk nanobubble and relevant applications: a review. J Clean Prod Nov 2023. https://doi.org/10.1016/j.jclepro.2023.139153
[6] Zhou L, Wang S, Zhang L, Hu J. Generation and stability of bulk nanobubbles: a review and perspective. Curr Opin Colloid Interface Sci Jun 2021. https://doi.org/10.1016/j.cocis.2021.101439
[7] Ouyang L, Hansen HHWB, Cha H, Ji X, Zhang J, Li Q, Tan BH, Trinh QT, Nguyen NT, An H. A novel approach for nanobubble generation toward biomedical applications. Colloids Surf A Physicochem Eng Asp Nov 2024;700. https://doi.org/10.1016/j.colsurfa.2024.134773
[8] Zhang M, Seddon JRT, Lemay SG. Nanoparticle–nanobubble interactions: charge inversion and re-entrant condensation of amidine latex nanoparticles driven by bulk nanobubbles. J Colloid Interface Sci 2019;538:605–10. https://doi.org/10.1016/j.jcis.2018.11.110
[9] Michailidi ED, Bomis G, Varoutoglou A, Kyzas GZ, Mitrikas G, Mitropoulos AC, Efthimiadou EK, Favvas EP. Bulk nanobubbles: production and investigation of their formation/stability mechanism. J Colloid Interface Sci 2020;564:371–80. https://doi.org/10.1016/j.jcis.2019.12.093
[10] Tan BH, An H, Ohl CD. Stability of surface and bulk nanobubbles. Stab Surf Bulk Nanobubbles Jun 2021. https://doi.org/10.1016/j.cocis.2021.101428
[11] Li M, Ma X, Eisener J, Pfeiffer P, Ohl CD, Sun C. How bulk nanobubbles are stable over a wide range of temperatures. J Colloid Interface Sci 2021;596:184–98. https://doi.org/10.1016/j.jcis.2021.03.064
[12] Shi X, Xue S, Marhaba T, Zhang W. Probing internal pressures and long-term stability of nanobubbles in water. Langmuir 2021;37(7):2514–22, pMID: 33538170. https://doi.org/10.1021/acs.langmuir.0c03574
[13] Hassanloo H, Wang X. Combustion mechanism of nanobubbled dodecane: a reactive molecular study. Fuel Oct 2024;374. https://doi.org/10.1016/j.fuel.2024.132486
[14] Hassanloo H, Wang X. Combustion mechanism of nanobubbled dodecane: a reactive molecular study. Fuel 2024;374:132486. https://www.sciencedirect.com/science/article/pii/S001623612401634X.
[15] Hassanloo H, Wang X. Unveiling the inherent properties and impact of ultrafine nanobubbles in polar and alcoholic media through unsupervised machine learning and atomic insight. Int J Thermofluids 2024;23:100734. https://doi.org/10.1016/j.ijft.2024.100734. https://www.sciencedirect.com/science/article/pii/S2666202724001769.
[16] Biswal A, Kale R, Teja GR, Banerjee S, Kolhe P, Balusamy S. An experimental and kinetic modeling study of gasoline/lemon peel oil blends for PFI engine. Fuel 2020;267:117189. https://doi.org/10.1016/j.fuel.2020.117189. https://www.sciencedirect.com/science/article/pii/S0016236120301848.
[17] Biswal A, Kale R, Balusamy S, Banerjee R, Kolhe P. Lemon peel oil as an alternative fuel for GDI engines: a spray characterization perspective. Renewable Energy 2019;142:249–63. https://doi.org/10.1016/j.renene.2019.04.087
[18] Kale R, Banerjee R. Investigation of macroscopic as well as microscopic spray behavior of multi-hole GDI injector under engine like hot injector body conditions. In: SAE technical papers, vol. 2018-April. SAE International; 2018. https://doi.org/10.4271/2018-01-0280
[19] Oh SH, Han JG, Kim JM. Long-term stability of hydrogen nanobubble fuel. Fuel 2015;158:399–404. https://doi.org/10.1016/j.fuel.2015.05.072
[20] Oh SH, Yoon SH, Song H, Han JG, Kim JM. Effect of hydrogen nanobubble addition on combustion characteristics of gasoline engine. Int J Hydrogen Energy 2013;38:14849–53. https://doi.org/10.1016/j.ijhydene.2013.09.063
[21] Nakatake Y, Kisu S, Shigyo K, Eguchi T, Watanabe T. Effect of nano air-bubbles mixed into gas oil on common-rail diesel engine. Energy 2013;59:233–9. https://doi.org/10.1016/j.energy.2013.06.065
[22] Gobinath S, Senthilkumar G, Beemkumar N. Air nanobubble-enhanced combustion study using mustard biodiesel in a common rail direct injection engine. Energy Sources Part A Recovery Utilization Environ Eff 2019;41:1809–16. https://doi.org/10.1080/15567036.2018.1549159
[23] Xuan R, Guo L, Cai N, Sun W, Yan Y, Zhang H, Chen Y, Wang H, Zhang J, Ge Y. Study on spray characteristics of micro-nano bubble premixed fuel. Fuel May 2024;363. https://doi.org/10.1016/j.fuel.2024.131035
[24] Jedelský J, Jícha M. Spray characteristics and liquid distribution of multi-hole effervescent atomisers for industrial burners. Appl Therm Eng 2016;96:286–96. https://doi.org/10.1016/j.applthermaleng.2015.11.079
[25] Sun C, Ning Z, Qiao X, Lv M, Li Y, Zhao J, Wang X. Study on effervescent spray morphology based on internal gas-liquid two-phase flow patterns. Eur J Mech B Fluids 2019;74:123–38. https://doi.org/10.1016/j.euromechflu.2018.10.025
[26] Babu KS, Amamcharla JK. Generation methods, stability, detection techniques, and applications of bulk nanobubbles in agro-food industries: a review and future perspective. Crit Rev Food Sci Nutr 2023. https://doi.org/10.1080/10408398.2022.2067119
[27] Han G, Chen S, Su S, Huang Y, Liu B, Sun H. A review and perspective on micro and nanobubbles: what they are and why they matter. Miner Eng Nov 2022. https://doi.org/10.1016/j.mineng.2022.107906
[28] Zhou ZA, Xuand Z, Finch JA. On the role of cavitation in particle collection during flotation-a critical review, Tech. rep. (1994).
[29] Meegoda JN, Hewage SA, Batagoda JH. Stability of nanobubbles. Environ Eng Sci 2018;35:1216–27. https://doi.org/10.1089/ees.2018.0203
[30] Montazeri SM, Kalogerakis N, Kolliopoulos G. Effect of chemical species and temperature on the stability of air nanobubbles. Scientific Rep Dec 2023;13. https://doi.org/10.1038/s41598-023-43803-6
[31] Lee JI, Huh HS, Park JY, Han JG, Kim JM. Coarsening behavior of bulk nanobubbles in water. Sci Rep Dec 2021;11. https://doi.org/10.1038/s41598-021-98783-2
[32] Ahmed AKA, Sun C, Hua L, Zhang Z, Zhang Y, Zhang W, Marhaba T. Generation of nanobubbles by ceramic membrane filters: the dependence of bubble size and zeta potential on surface coating, pore size and injected gas pressure. Chemosphere 2018;203:327–35. https://doi.org/10.1016/j.chemosphere.2018.03.157
[33] Ushikubo FY, Enari M, Furukawa T, Nakagawa R, Makino Y, Kawagoe Y, Oshita S. Zeta-potential of micro- and/or nano-bubbles in water produced by some kinds of gases. IFAC Proc Vol 2010;43(26):283–8, 3rd IFAC Conference in Modelling and Control in Agriculture, Horticulture and Post-Harvest Processing - Agricontrol. doi:https://doi.org/10.3182/20101206-3-JP-3009.00050
[34] Antonov DV, Fedorenko RM, Strizhak PA. Micro-explosion phenomenon: conditions and benefits. Energies 2022;15(20). https://www.mdpi.com/1996-1073/15/20/7670.
[35] Watanabe H, Okazaki K. Visualization of secondary atomization in emulsified-fuel spray flow by shadow imaging. Proc Combust Inst 2013;34(1):1651–8. https://doi.org/10.1016/j.proci.2012.07.005
[36] Gao H, Zhang F, Zhang Z, Wang E, Liu B. Experimental investigation on the spray characteristic of air-assisted hollow-cone gasoline injector. Appl Therm Eng 2019;151:354–63. https://doi.org/10.1016/j.applthermaleng.2019.02.029